Int. J. Electrochem. Sci., 15 **(2020)** 2243 – 2260, doi: 10.20964/2020.03.72

International Journal of
ELECTROCHEMICAL
SCIENCE
www.electrochemsci.org

Electrochemical Corrosion Behaviour of Different Cu-Base Alloys in Concentrated LiBr Solutions: Part I - Cu/10Ni and Al-Bronze Alloys

A. E. El Melleigy[1], *A. A. El Warraky*[1], *Sh. E. Abd El hamid*[1] *and El-Sayed M. Sherif*[1,2,*]

[1] Electrochemistry and Corrosion Laboratory, Department of Physical Chemistry, National Research Centre, El-Behoth St. 33, Dokki, Cairo 12622, Egypt.
[2] Center of Excellence for Research in Engineering Materials (CEREM), King Saud University, P.O. Box 800, Al-Riyadh 11421, Saudi Arabia.
[*]E-mail: esherif@ksu.edu.sa; emsherif@gmail.com

Received: 1 October 2019 / *Accepted:* 8 January 2020 / *Published:* 10 February 2020

The behaviour of Cu\10Ni and Al-bronze in different concentrations of Li Br solution has been studied using electrochemical measurements and surface analysis techniques. Potentiodynamic polarization measurements found that there is no any type of local attack observed for Cu/10Ni at 4M LiBr and one step recorded at low current density as a result of the formation of the inner doped Cu_2O with Ni. The hysteresis loop area was appeared at very small current density in the second anodic cyclic polarization in case of Cu/10Ni of solution containing the soluble corrosion product (SCP) of each of Cu/10Ni, Cu/30Ni, Cu/30Zn and Cu/7Al. This is due to the increase in the thickness of both the inward doped oxide film and the outer oxide film formation, which become protective enough to produce pitting attack at the weak points on the surface. In case of Cu/7Al, the inward doped Cu_2O cannot form and the general dissolution takes place. Surface analysis techniques using scanning electron microscopy (SEM) and energy dispersive X-ray spectroscopy (EDX) recorded an appearance for cavities or depressions in case of Cu/10Ni and Al-bronze. In 6 M LiBr Cu\10Ni, in presence of SCP of Al-bronze, Cu\10Ni recorded a large hysteresis loop area at very low current density, which is larger than that recorded at 4M LiBr due to the increase of the concentration of SCP. The EDX analysis of Cu\10Ni after treated for 120 min using current–time measurement indicated that inside the pits, Cu and Ni present on the surface with very small amount, while Br shows a higher value than outside and confirms the role of Br^- in the pitting attack. The mechanism of pitting corrosion of Cu/10Ni in concentered solution of LiBr is discussed. The dealuminification of the surface in case of Cu\7Al occurs either outside or inside the cavities.

Keywords: Cu-base alloys; corrosion; LiBr; potentiodynamic polarization; chronoamperometry

1. INTRODUCTION

In practice, lithium bromide heavy brines are widely used as absorbents for heating and refrigerating absorption systems that use a natural gas or steam as energy sources [1-9]. Although

lithium bromide has favorable thermo-physical properties, it can cause serious corrosion problems on metallic components of cooling systems and heat exchangers at absorption plants such as copper alloys, carbon steel, and stainless steel [10-13]. Some of disadvantages of LiBr/water mixtures are high corrosion rates at high temperature, low working pressure, and crystallization at high LiBr concentration [1].

Copper-nickel alloys are one of the main sources of marine piping materials and heat exchanger tubing materials due to their good thermal conductivity, mechanical workability, and resistance to sea water corrosion. The good resistance to corrosion is attributed to the formation of the protective corrosion product film on the surface of the alloys [14-17]. Their corrosion rates decrease with increasing Ni content up to around 40 wt% then remain approximately constant. The efficacy of Ni additions to a passive reaction is attributed to occur at a critical electron to atom ratio at which the ″d″ shell becomes unfilled. The tendency for flaking of corrosion product on bare copper sheet and copper-based alloys is influenced by the alloying elements in the substrates. Authors explained the anti-corrosion superiority of the copper-nickel alloy over that of pure copper in terms of the defective semi-conductor property of the Cu_2O film on the copper-base alloys [18,19]. They presume that nickel were incorporate into the Cu_2O film, occupied cation vacancies, and reduced the number of cation vacancies and thus increased the corrosion resistance.

The corrosion behaviour of copper and copper alloys in different concentration of LiBr were studied by the same authors [19-22] using different electrochemical measurements and surface analysis techniques. The results of these studies [19-22] explained the nature and conditions of film formation, the composition, and the difference between the passive film, the partial passive, and porous film. It is well known that Cu alloys are used in refrigeration system, which used LiBr\H_2O heavy brine as absorbent in a closed circuit. By times, a soluble Cu corrosion product become more concentrated in LiBr fluid. In the light of the above, this statement has been adopted to explain the composition and formation mechanism of the corrosion product film on Cu/10Ni and Al-bronze alloys in different concentration of LiBr solutions using electrochemical measurements and surface analysis techniques. The study is extended to show the effect of the SCP on the dissolution of the two alloys.

2. EXPERIMENTAL PROCEDURES

The alloys selected for this investigation were made from Cu/10Ni, Cu/30Ni, Cu/30Zn and Al-bronze, and were welded to thick Cu wires for electrical connections. Before each experiment the electrodes surface was abraded with metallographic emery paper of increasing fineness down to 1000 grit. The abraded electrodes then were washed with running bi-distilled water, degreased by rubbing with cotton soaked with acetone, rewashed with running bi- distilled water and dried between filter papers. Details of electrochemical measurements, surface analysis techniques, solution preparation and other experimental methods were described previously [22].

An electrochemical cell made of pyrex glass, with three electrodes; a saturated calomel electrode was used as a reference electrode, a platinum foil was employed as a counter electrode, and

the working electrode was the tested alloys, respectively. The working electrode that was exposed to the electrolytic solution had the dimensions of 1 cm x 1 cm and total area of 1 cm^2.

Measurements were performed using a PS6 Meinsberger Potentiostat/ Galvanostat, (Germany). The potentiodynamic cyclic polarization curves were recorded in different concentration of LiBr. Before polarization measurements, the sample was kept at -600 mV versus saturated calomel electrode (SCE) for 20 min in the test solution to reduce the oxides on the sample surface. The potentiodynamic cyclic polarization test was carried out by scanning the potential of the electrode from -600 mV towards noble values up to 800 mV using a scanning rate of 1 mV/S and reversed again to the backward direction with the same scan rate. The second cyclic of the anodic polarization was taken by exchanged the sample only by a new one in the same solution which contains dissolved corrosion product of the first sample.

Current - time tests were achieved by the application of a constant potential value, (-200 mV), for 120 min. Some of the samples were taken for surface analysis, where the samples were cleaned in bidistilled water for 30 min using ultrasonic vibration and dried between fibreless tissues and immediately introduced into the vacuum chamber of scanning electron microscope (scanning electron microscope JXA-840A electron probe microanalyzer (SEM), JEOL equipped with energy dispersive X-ray (EDX), JXA-840A Electron probe microanlyzer JEOL. Furthermore, analysis of the solution was performed using a Perkin - Elmer type 2380 atomic absorption spectrophotometer.

3. RESULTS AND DISCUSSION

3.1. Cyclic potentiodynamic polarization

The anodic potentiodynamic cyclic polarization curves of Cu/10Ni in different concentration of 4, 6 and 9 M LiBr have been studied. In all our polarization measurements, the anodic forward direction is represented by the bold line, while the backward direction is represented by the narrow line. Figure 1(a) displays the polarization curve for Cu/10Ni alloy in 4 M LiBr, which shows that there is no hysteresis loop area recorded, which reflected the absence of any type of local attack such as pitting. The curve of the above figure represented only the appearance of one step at -340 mV, which recorded at very low current density of 0.04 mA/cm^2. This occurs as a result of the formation of a doped Cu_2O [22]. By exchanged the sample only by a new one of Cu\10Ni, the second cyclic of the anodic polarization of Figure 1(b) was taken in the same solution, which contains dissolved corrosion product of the first sample of Figure 1(a). The sample was changed by a new one, to make the second cycle and to avoid the decrease in the area owing to the aggressiveness of Br^- ion concentration. Figure1(b) represented that a hysteresis loop area was recorded at pitting potential (E_{Pit}) = -135mV and pitting current (I_{Pit}) = 0.05 mA/cm^2. By changing the dissolved product from alloy to another, the curves of Figure 1(c-e) was taken for Cu/10Ni in 4M LiBr containing the SCP; this SCP is the corrosion products that has resulted from the first cycle of anodic polarization of each of Cu/30Ni, Cu/30Zn and Cu/7Al, respectively.

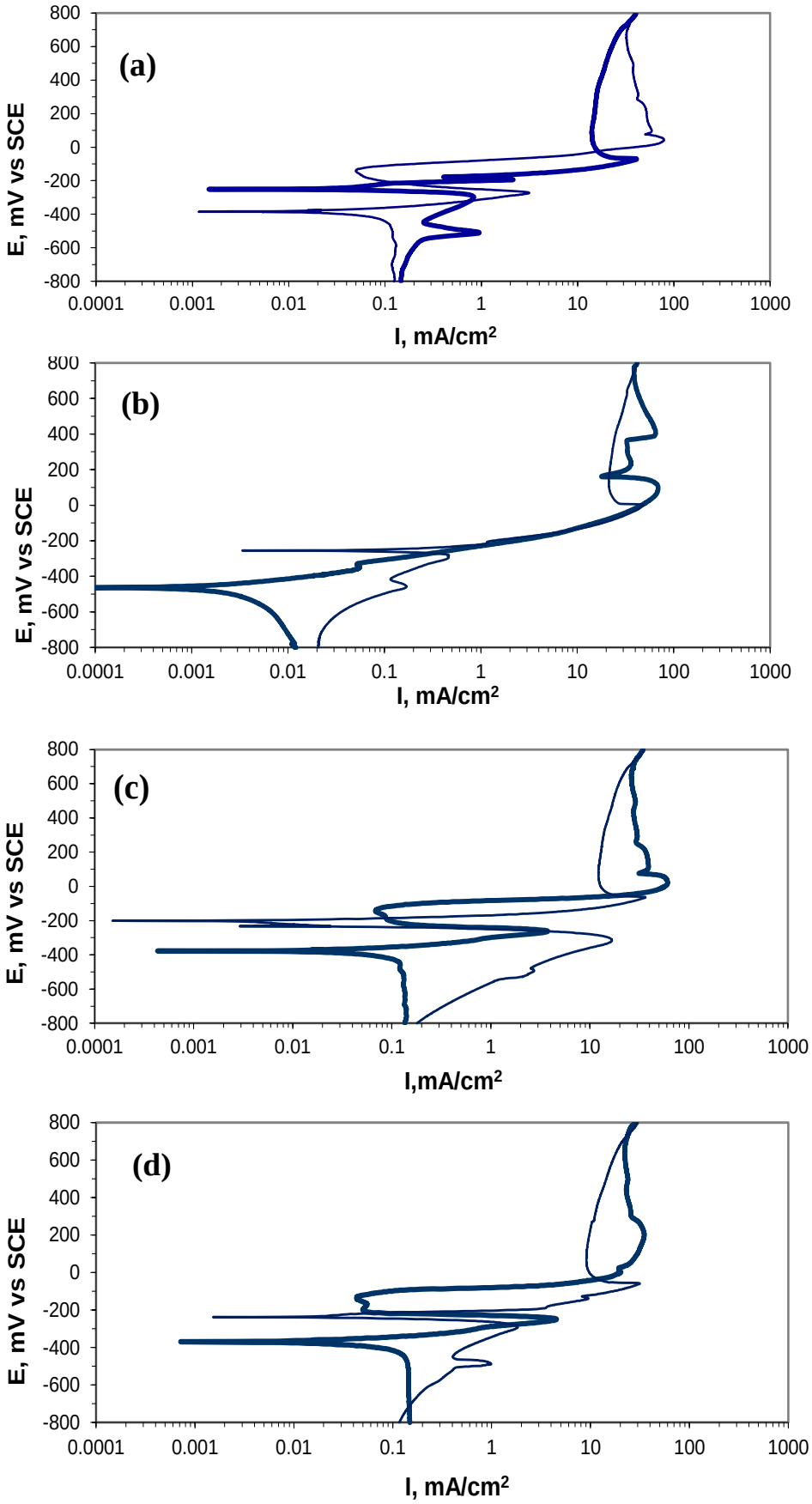

Figure 1. Potentiodynamic polarization for Cu/10 Ni in 4 M LiBr (a) without SCP and with SCP of each of (b) Cu/10Ni (c) Cu/30Ni (d) Cu/30Zn (e) Cu/7Al alloys, respectively.

The curves of Figure 1(c-e) represented the appearance of hysteresis loop area at very small current densities of 0.05 mA/cm^2 and E_{Pit} = -135mV depending on the SCP of the studied alloy as shown in Figure 1(b-e) and Table 1. On the other hand, a positive shift of corrosion potential (E_{Corr}) of more than 90 mV is observed for the second cycle in comparison with E_{Corr} of the first cycle (blank) and different parameters are recorded in Table 1. This can interpret by the inhibiting effect due to formation of a protective film of corrosion product which decreases the anodic reaction in terms of the mixed potential theory [23]. By increasing the concentration of LiBr to 6M, Figure 2 (a) was produced. The curve of Figure 2(a) represented the same behaviour as recorded in 4M LiBr where, a small shift to more negative potential of E_{Corr} and maximum current (I_{Max}) are recorded. Figure 2(b) represents the second anodic cyclic polarization of Cu/10Ni in the SCP of Al-bronze of 6 M LiBr. A larger hysteresis loop area is produced where, a remarkable passive behaviour over a wide range of potential from -350 mV to +100 mV, and the current density decreased to about 0.01 as shown in Figure 2(b) and Table 1.

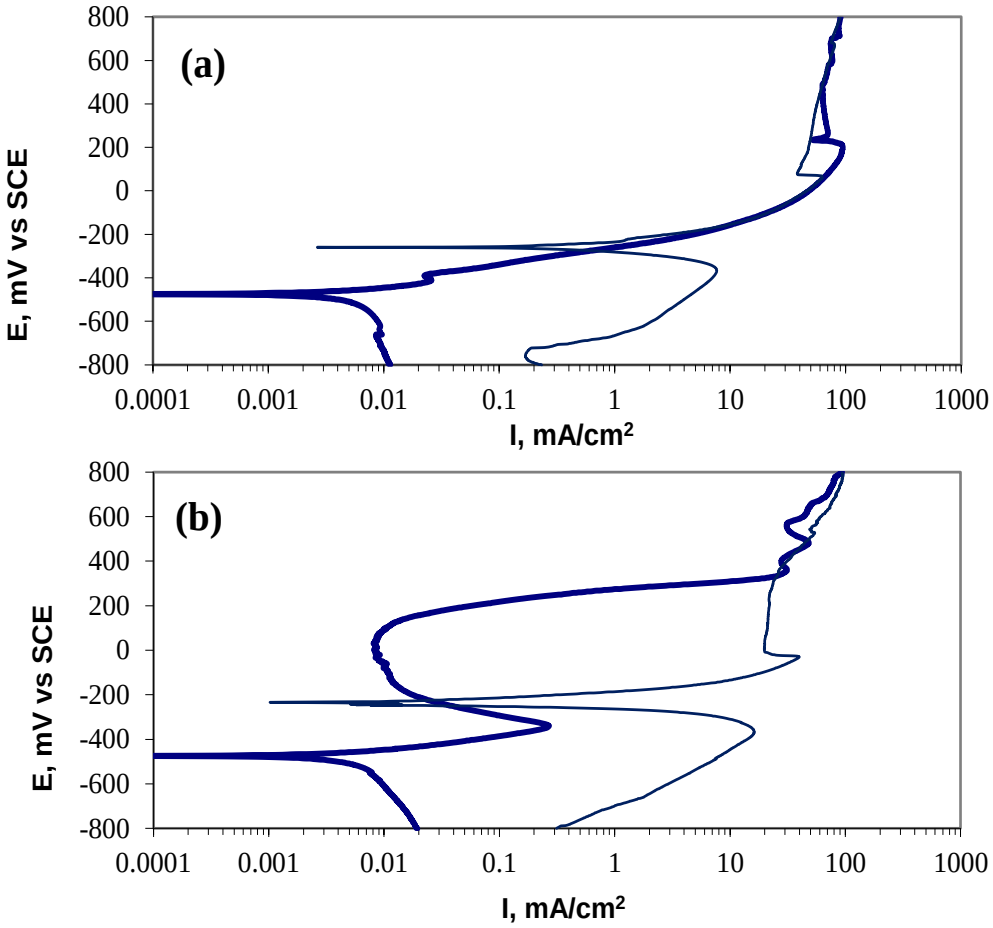

Figure 2. Potentiodynamic polarization for Cu/10Ni in 6 M LiBr (a) without SCP and (b) with SCP of Cu/7Al alloy.

The cyclic anodic potentiodynamic polarization curves of Al-bronze in 4 M LiBr are shown in Figure 3(a). This figure is similar to that recorded in the case of Cu/10Ni as shown in the resuls. The only difference is the no detection of the step that recorded at low current density in case of Cu/10Ni.

A second cycle of Al-bronze was performed in the same solution of the first cycle by changing the sample only which produces Figure 3(b). As previously mentioned, the sample had to be changed to avoid the decrease of sample area owing to the aggressiveness of Br^-. The first cyclic of Cu/10Ni, Cu/30Ni and Cu/30Zn alloys, which is followed by the second cyclic of Al-bronze in the same solution are shown in Figure 3(c-e), respectively. It is observed that the curves of the figures are not similar to that recorded in case of Cu/10Ni. However, the hysteresis loop area that was previously recorded in the case of Cu/10Ni is disappeared as a result of the absence of any localized attack. This occurs because Al in Al-bronze cannot play the rule of Ni in Cu/10Ni alloy and the dissolution of Al -bronze takes place via general corrosion not localized attack.

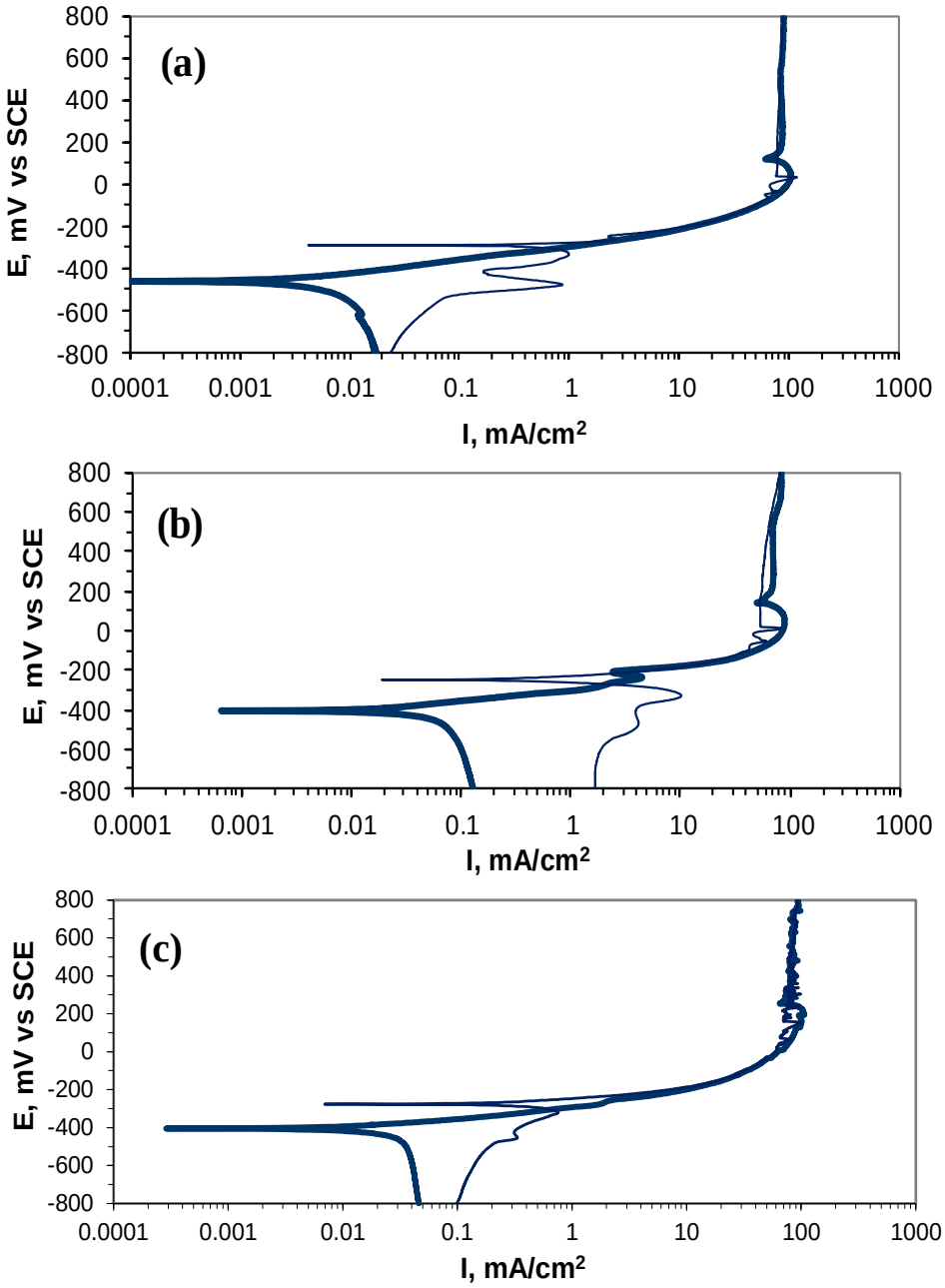

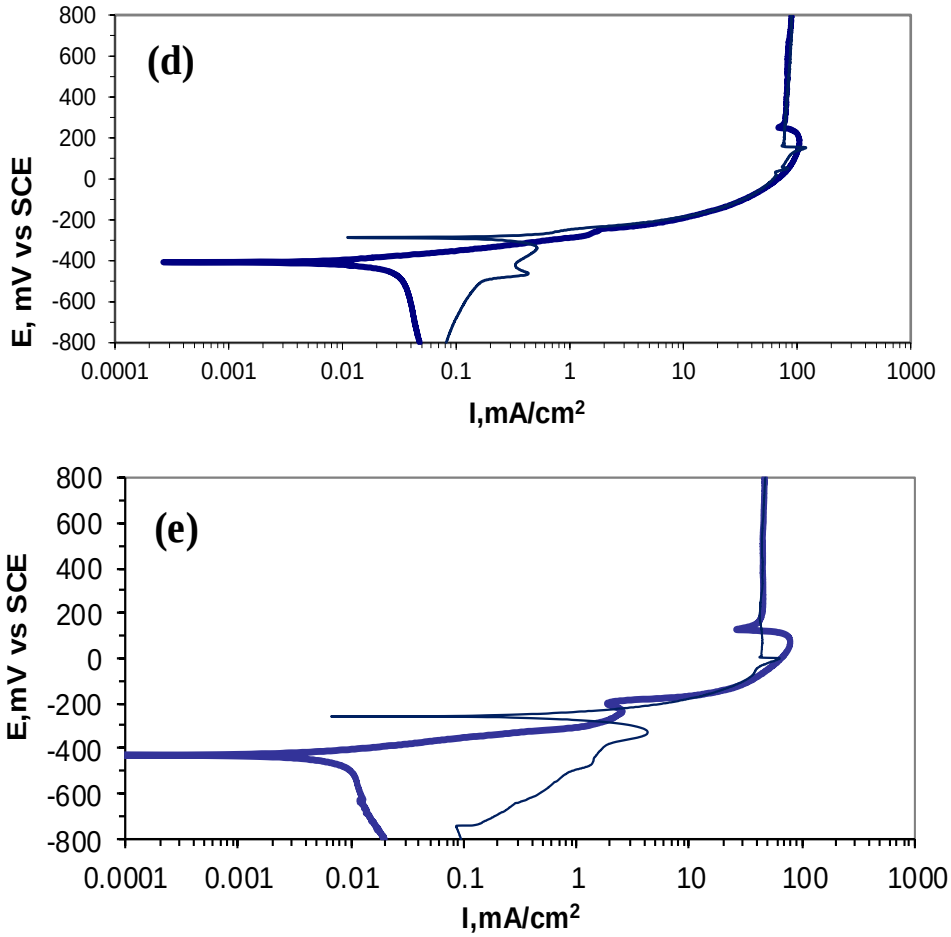

Figure 3. Potentiodynamic polarization for Cu/7Al in 4M LiBr (a) without SCP and with SCP of each of (b) Cu/7Al (c) Cu/10Ni (d) Cu/30Ni (e) Cu/ 30Zn alloys.

Table 1. Corrosion parameters obtained from the polarization curves shown in Figure 3 for the Cu/10Ni alloy after its immersion in the solutions that have the corrosion products of Cu/10Ni, Cu/30Zn, Cu/7Al, and Cu/30Ni alloys after their exposure to 4M LiBr solution.

Corrosion Product	E_{Corr} / mV	E_{baek} / mV	E_P / mV	I_P / µA	E_{Pit} / mV	I_{Pit} / µA	E_{RP} / mV	I_{RP} / µA	E_{Pit}-E_{RP} / mV
Cu/10Ni in 4M LiBr	-460	-265	-340	0.04	—	—	—	—	—
In solution of Cu/10Ni	-390	-250	-270	3.00	-135	0.05	-220	0.12	85
In solution of Cu/30Zn	-370	-240	-250	4.55	-130	0.04	-240	0.08	110
In solution of Cu/7Al	-375	-240	-265	1.98	-235	0.06	-240	0.3	5
In solution of Cu/30Ni	-380	-200	-260	2.60	-140	0.06	-200	0.08	60

3.2. Current – time measurement

The variations of current density of, Cu/10Ni and Cu /7Al in 4 M LiBr at -200 mV are shown in Figure (4), the concentration of 4 M was taken only due to its similarity with 6 and 9 M. The general features that can be distinguished from these figures are: For the two alloy studied, the initial current densities decrease at the moment of polarization which is followed by a steady state in the current densities to the value of 1.5 mA and 8 mA for Cu/10Ni and Cu/7Al, respectively. A higher steady state in the current density of 7.1 mA/cm^2 is occurring in case of Al- bronze as shown in Figure (4) and the lower is recorded with Cu/10Ni of 0.2 mA/cm^2. These results depend on the film formed on each alloy (see SEM and EDX analyses).

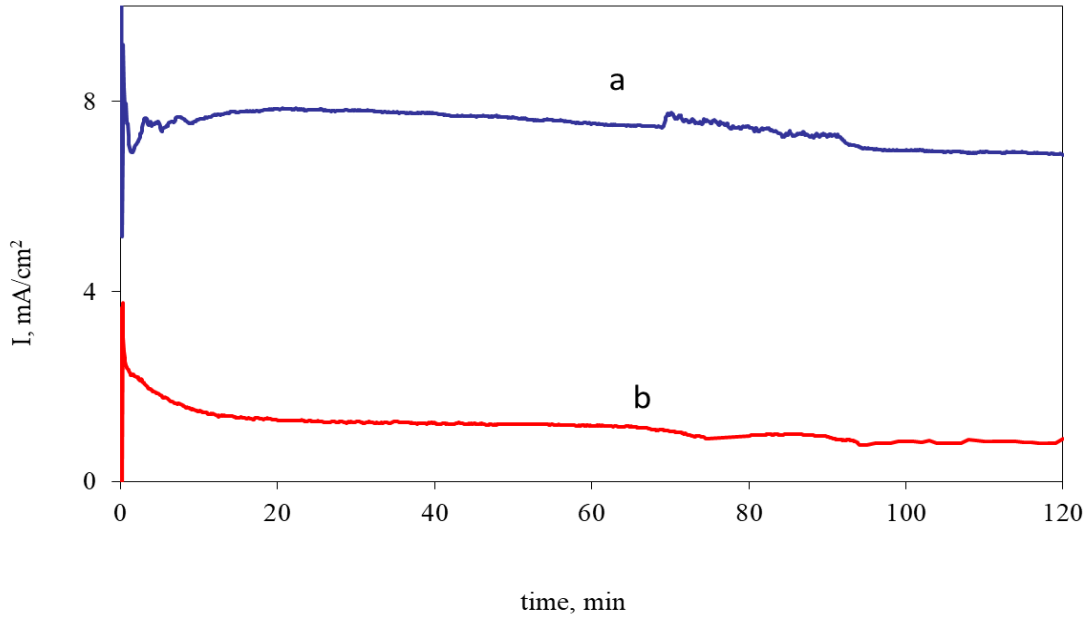

Figure 4. Current time in 4 M LiBr at constant potential of -200 mV of (a) Cu/7Al (b) Cu/10Ni alloys.

3.3. surface analysis examination

The surface examination of the film formed after equilibration of the Cu/10Ni in 4MLiBr at constant potential of -200mv for 120min at the end of experiment of Figure (4) is performed using SEM technique. The picture of Figure (5) shows a large number of pit initiation which is accompanied by a small number of pitting propagation. This occurs as a result of formation of a protective film of doped Cu_2O on the Cu/10Ni alloy surface [22]. This is due to incorporation of nickel ions in the Cu_2O film which enhances the ionic and electronic resistance of the film where, nickel ion occupies the cation vacancies of Cu^+. Accordingly, the oxide film formed becomes more compact and passive and pitting attack occurs at small location area, which is weak in the passive film. The appearance of pitting corrosion as shown by the SEM of Figure (5) is not in agreement with the results obtained from the anodic potentiodynamic polarization of Figure 1(a), and current –time of Figure (4). This confirmed by the EDX analysis of the surface of Cu/10Ni after the above treatment which is shown in

Figure 6 (a,b) SEM and EDX analysis were preformed after the first cyclic to clarify the composition of the film formed on the alloy surface and to show the role of the insoluble corrosion product in the mechanism of dissolution of Cu/10Ni in solution of 4 M LiBr at -200 mV.

It was possible though the versatility of the spectrometer to direct the electron beam of the EDX to specific points on the film surface in order to identify the constituent elements. The EDX analysis was performed both inside and outside pits. The spectra shown in Fig 6 (a,b) and are representative of this type of analysis for film formed on Cu/10Ni in 4M LiBr solution at -200 mV for 120 min. Several facts could be drowning out depending on the location of analysis either inside or outside pits (regular surface).

(a) The carbon signal is present and its atomic conc. % (at. %) is 33.99 outside in comparison with inside the pit which show a very high intensity and also high atomic conc. % of 68.43 as in Figure 6 (a,b). It is clear that the surface outside and inside pits was covered by carbon because the surface of the alloy at -200mV was active enough to adsorb carbon from the atmosphere as reported previously in case of NaCl [24].

(b) Oxygen outside the pit recorded is lower value of 11.21 at. % in comparing with that inside which show that Oxygen is 16.12 at. % as shown in Figure 6 (b).

(c) The signal of Br and its ratio inside pit are higher than outside, where its ratio was 0.91 at. % inside and 0.25 at. % outside.

(d) The measured at. % for Cu and Ni outside the pit obtained from Figure 6 (a) was 49.06 and 5.47, respectively, which were higher than inside the pit. Where, the at. % recorded for Cu was 13.04 and Ni was 1.5 and its ratio was lower than that in the alloy matrix. This means that the enrichment of Ni takes place on the surface of the alloy.

In the light of the above results, Cu and Ni show enhanced signals outside the pit. These aggregated Cu and Ni peaks and concentration outside are due to the thin nature of Cu and Ni oxide, which allows the electron beam of EDX to detect Cu and Ni from the formed oxide film and from the metallic of the substrate. The Cu and Ni signals detected inside the pit show a small peak and its concentration is also very small. This occurs as a result of the presence of a massive carbon species, which are very thick and also the signal of Figure 6 (b) shows that the oxygen peak is always larger for inside than outside pit. Another fact for the presence of carbon in associated with reduced level of Cu and Ni in the pits may explanted on the bases of compilation between adsorption of carbon and formation NiO and Cu_2O in LiBr solution. These facts are detected previously in case of Ag, Cu and Cu alloy [25,26] in chloride, which used more recent surface analysis techniques such as XPS and AES and concluded that some defective points of the alloy surface are characterized by shallow depressions or cavities. In these depressions some sort of massive carbon species is deposited which prevent the formation of Cu_2O or NiO in the depressions, the author [25] also concluded that where cavities represent a rout by which the solution oxygen keeps in contact with the alloy metal oxide interface, to maintain the potential of the system at metal/metal oxide potential. These conclusions are in agreement with our results where inside pit carbon and oxygen are detected with higher ratio in compression with outside pits and the same of oxygen is from solution while carbon adsorbed at active site of depression or cavities, from atmospheric hydrocarbons. Other author [27,28] reported that free carbon can be formed from solutions containing sulphide, cuprous compound, either organic or

inorganic. Also found that, carbon in the film increases its electronic conductivity and accordingly the film become has good catalytic property of oxygen reduction. As a consequence, the carbon which detected in our results has the same property. Moreover, the micrograph of Figure 5(c) for Cu/10Ni show that the surface was suffered from pitting initiation and some of propagation. Figure 5(c), was taken at higher magnification of 1500x also show the formation of different phases and there is an attack on the grain boundary which is called intergranular corrosion.

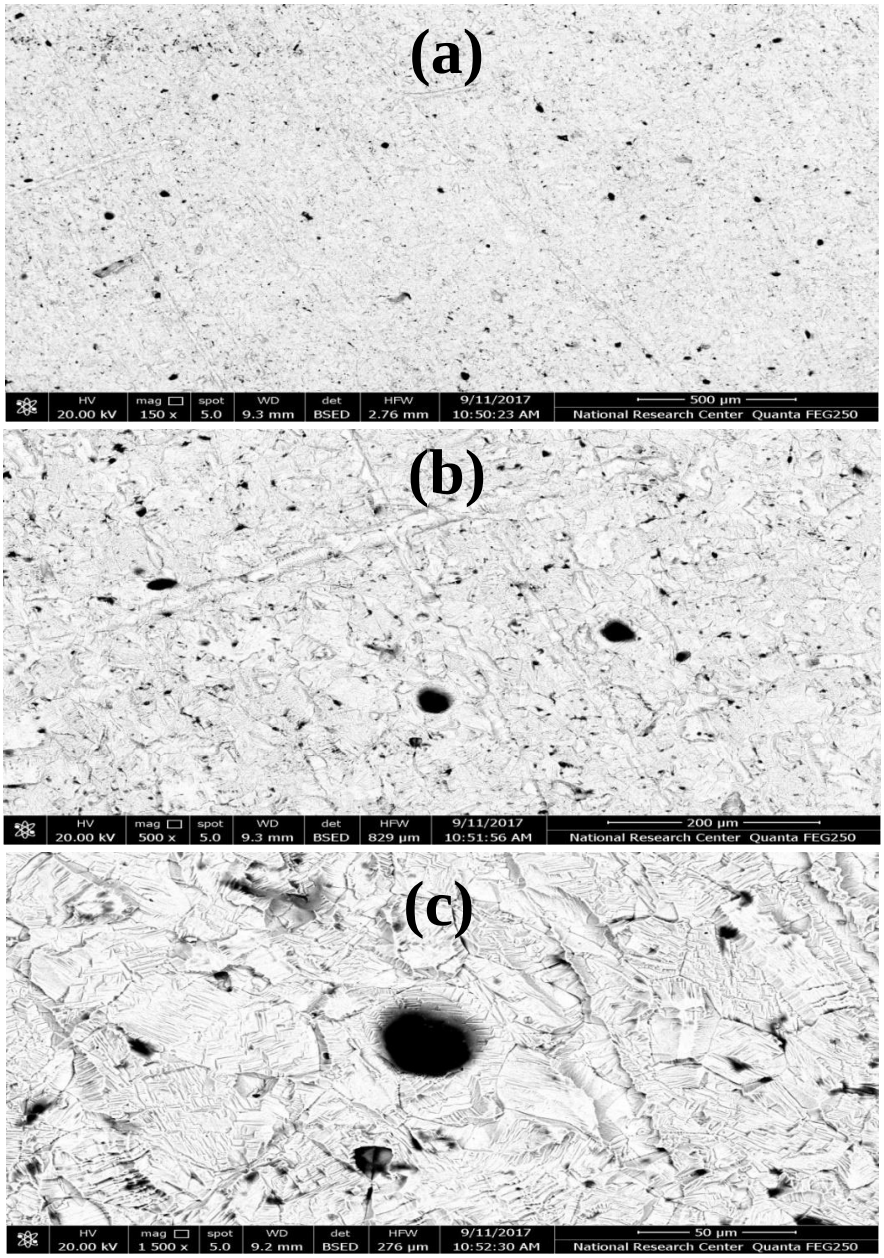

Figure 5. SEM micrographs obtained for Cu/10Ni alloy in 4 M LiBr solution at -200 mV.

The EDX analysis inside pit indicated that Cu and Ni present on the surface with very small amount in comparison with outside pit while Br show a higher value inside pit than outside which

confirm the role of Br^- in the pitting attack. The presences of O with a higher value than Br outside the pit suggest that the surface is covered mainly with a Cu_2O and NiO. This is in agreement with Jiang etal. [14] who found that after treated of Cu/10Ni in NaCl a Cu_2O formed can be divided into the outer layer of Cu_2O which precipitation from the dissolved species of copper and the inner layer formed by the inward growth of Cu_2O film. The inner layer is more protective because it is more compact than the outer. On the other hand, Ni on the surface exists with a higher ratio in comparison with that in the alloy matrix, in the form of both oxidized state as (NiO and $Ni(OH)_2$) and in metallic state. The author [14] hypothesized that the presence of Ni in the film is probably as a result of a disproportionately high rate of dissolution of Cu. While, NiO in the inner layer is due to transformation from Cu_2O into microcrystal NiO with Cu_2O lattice where the concentration of Ni incorporation reaches a certain value.

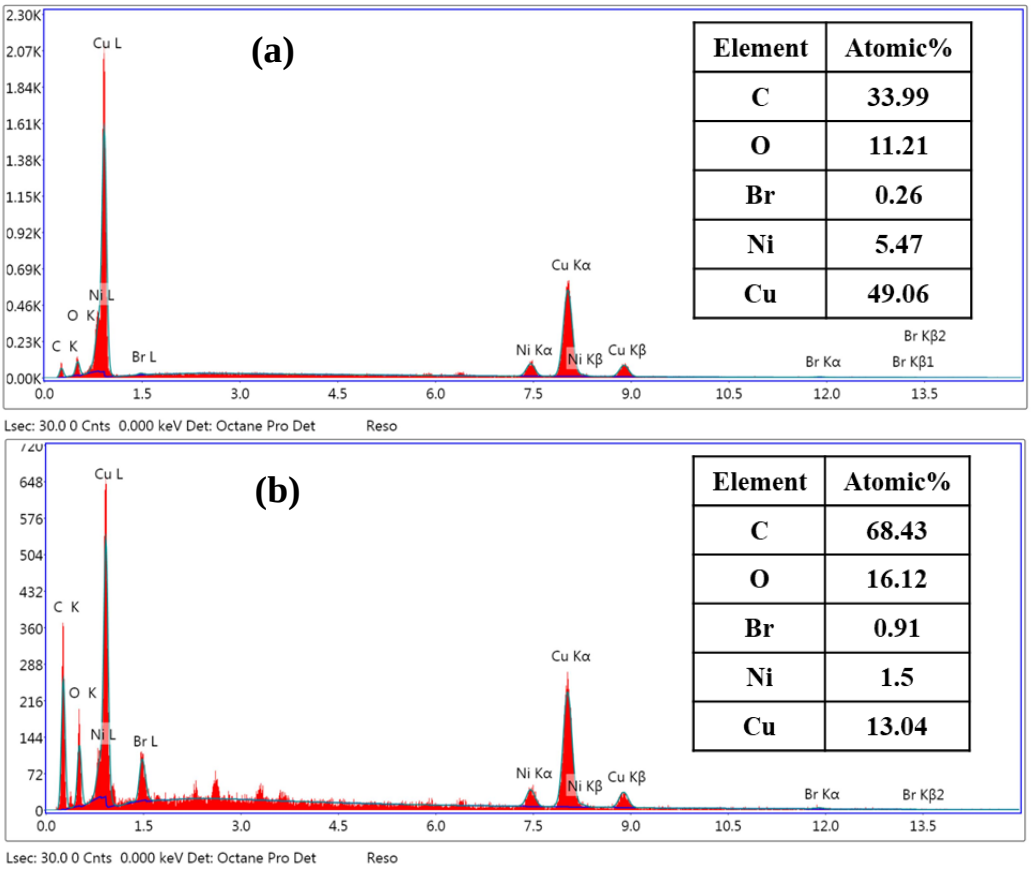

Figure 6. EDX analysis for Cu/10Ni in 4 M LiBr at -200 mV, (a) outside pits and (b) inside pits.

It is believed that the detected $NiO/Ni(OH)_2$ in the film formed is contributed in the higher resistance of the alloy. The above conclusion gives another confirmation on the formation of Cu_2O and the corrosion resistance of Cu/10Ni alloy in 4M LiBr is attributed to the thin compact inner film of Cu_2O and incorporating $Ni^{2+}$and Ni^{3+} beneath a thick film of porous outer layer of Cu_2O.

Many authors [16,19-22,29] showed that general dissolution of Cu and Cu alloys occurs in presence of chloride ions. This is in agreement with the present results as recorded in Figure (1a) where;

$Cu = Cu^{+} + e$ (1)

$Cu^{+} + Br^{-} = CuBr$ (2)

$CuBr + Br^{-} = CuBr_2^{-}$ (3)

$2CuBr = Cu + CuBr_2$ (4)

$CuBr_2 + Ni = NiBr_2 + Cu$ (5)

And the cathodic reaction is;

$O_2 + 2H_2O + 4e^{-} = 4OH^{-}$ (6)

Or $CuBr_2^{-}$ may be formed by Eq. (7) and as previously proposed [30-34] in case of NaCl where;

$Cu^{+} + 2Br^{-} = CuBr_2^{-}$ (7)

The precipitation of Cu_2O occurs as;

$2CuBr_2^{-} + 2OH^{-} = Cu_2O + H_2O + 4\ Br^{-}$ (8)

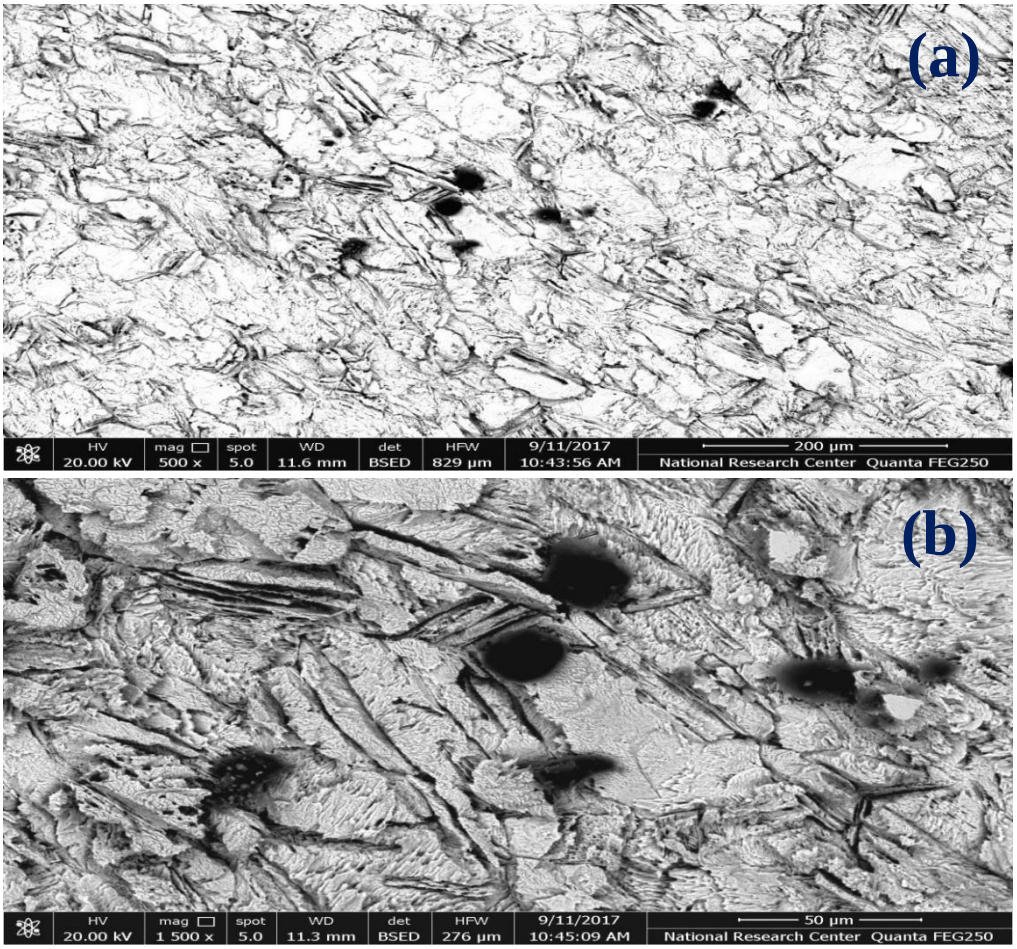

Figure 7. SEM images obtained for Cu/7Al alloy in 4 M LiBr solution at -200 mV.

As increasing the $CuBr_2^-$ by time in solution, Cu_2O is formed with a slow rate by precipitation. According in our result $CuBr_2^-$ is present from the first cyclic and when change the sample only in the second cycle in the same solution, $CuBr_2^-$ acts in the formation of Cu_2O as shown in Eq. (8). So that the oxide film becomes more thick enough to protect the alloy from the general dissolution, while localized attack occurs at the weak point of the oxide film formed as represented later in the mechanism of pitting.

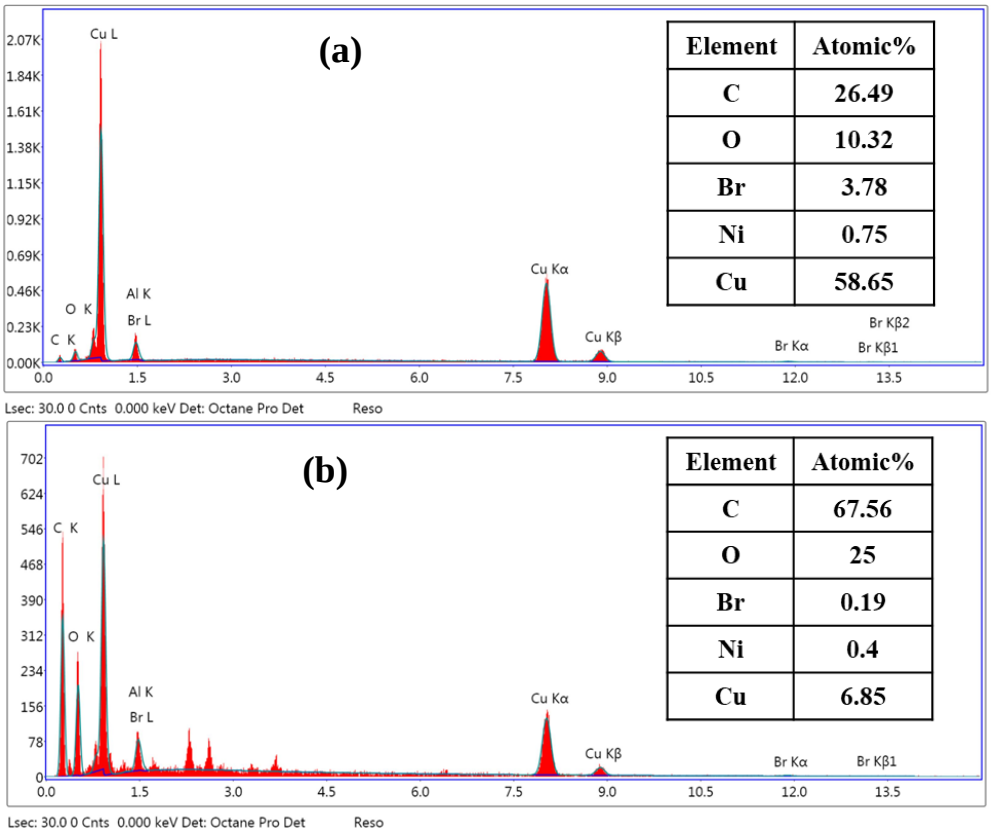

Element	Atomic%
C	26.49
O	10.32
Br	3.78
Ni	0.75
Cu	58.65

Element	Atomic%
C	67.56
O	25
Br	0.19
Ni	0.4
Cu	6.85

Figure 8. EDX analysis for Cu/7Al in 4 M LiBr at -200 mV, (a) outside cavity and (b) inside cavity.

The surface examination of the film formed of Al-bronze after treatment in 4M LiBr at constant potential of -200 mV for 120 min is examined using SEM. The photograph of Figure (7) show a five black spots which is called cavity and not pit as shown previously in Figure (8) and as discussed latter. The photograph also recorded that the surface has different type of grains such as equiaxed grain and needled or platelet like grain. The description of these black spots is a cavities or depression and not a pits as recorded in case of Cu/10Ni due to different facts. The first fact is the non-detection of any hysteresis loop area following cyclic anodic polarization of Figure 3(a). The curve of Figure (4) also not recorded any oscillation or fluctuation in the current density, the non-detection of the step at very small current density as recorded in case of Cu/10Ni confirm that Al in Al- bronze cannot play the role of Ni in Cu/10Ni alloy. The second fact is related to the higher current density of 7.1 mA recorded as in Figure 3(a), which proved that the oxide film formed is not passive and cannot satisfy the rule of pitting corrosion. The third fact is recorded using EDX analysis of Figure 8 (a,b), which show that the

concentration of Br recorded outside the cavity is higher than that recorded inside, which is in controversy with those recorded in case of Cu/10Ni. The forth fact also is the presence of carbon inside cavity with higher atomic conc. ratio of 67.58 in comparison with that of outside cavity of 26.49 at. % as shown in Figure 8 (a,b). This is nearly the same ratio recorded in case of Cu/10Ni. The last fact is related to the dealuminification of the surface either outside or inside the cavities as shown in Figure 8 (a,b).

3.4. Solution analysis

During the current-time experiment, small portions of 5 ml of the test solution was withdrawn each of 30 min and analyzed for their copper and nickel content using a Perkin-Elmer type 2380 atomic absorption spectrophotometer. The solution analysis of Table 2 represents that both Cu and Ni were present in solution at all the time of experiment of Figure (1a). The amount of Cu and Ni were increased by increasing the time of polarization. The ratio of copper /nickel in solution was smaller than the ratio of the bulk alloy at all polarization time. This indicates that the growth of the film on the surface and the dissolution of the Cu/10Ni alloy were controlled by diffusion [17,35]. This depends on the difference between the ionic radii of Cu^{+} and Ni^{2+} ions.

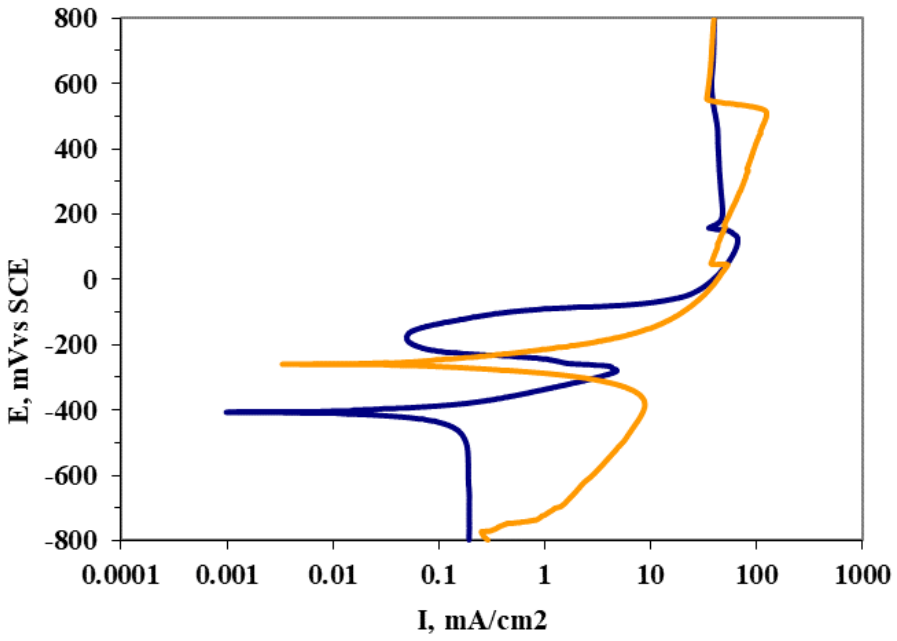

Figure 9. Potentiodynamic polarization for Cu/10 Ni in 4 M LiBr with SCP of Cu.

The ratio of copper/nickel were slightly increased in solution as increasing the time of polarization because the produced amount of Cu^{2+} from the moment of polarization (after 5 min) seems to have sufficient to go to solution despite to affinity to precipitate as copper metal through the galvanic reaction with nickel as represented in Eq. (5).

These results satisfy the simultaneous dissolution theory [36] which found that in case of acidified NaCl solution as increasing the concentration of Cu^{++} by time in solution the corrosion rate increased due to autocatalysis through the disproportion or catalytic reaction, which act in the formation of a CuBr film. This means that the rate of forward and backward reaction in equation (10) is increased;

$$2CuBr = Cu + CuBr_2 \quad (9)$$

This result is in agreement with anodic cyclic polarization of Figure (1b) where the second cycle show that the appearance of hysteresis loop area which cannot produce in the first cycle. This occurs where in the second cycle the concentration of Cu^{++} become enough to act in the dissolution through pilling attack along the weak point in the passive film. To confirm this result, another experiment was performed on Cu metal where the first cycle is Cu in 6M LiBr at -200 mV which is followed with the second cycle of Cu/10Ni in solution of the first cycle as represented in Figure (9) which recorded the hysteresis loop area. Accordingly, Cu^{++} is responsible on the pitting corrosion in Cu/Ni alloy beside the role of Br^- ion in the formation of oxide film as in Eq. (8) through hydrolysis. This satisfies the detection of pitting corrosion in the field. In the refrigeration system a closed cooling circuit of LiBr heavy brain is used where the system has different Cu and Cu alloys so that Cu^{++} ion in solution of LiBr can act in the dissolution of the chillier through pitting attack at the weak point on the passive film, of Cu_2O and NiO. Solution analysis in case of Cu/7Al cannot be performed because Al cannot go to the solution but it can be enriched at the interface as pointed out earlier by El Warraky and El Meleigy [37,38].

Table 2. Solution analysis after polarization for different periods of time in 4M LiBr solution.

Polarization time	Cu/10Ni alloy			
	Cu		Ni	
	ppm	%	ppm	%
After 5 min	0.5	62.5	0.3	37.5
After 30 min	3.9	92.8	0.3	7.2
After 60min	4.2	91.3	0.4	8.7
After 90 min	14.8	90.55	0.5	9.45
After 120 min	6.2	90.77	0.63	9.23

From the above studies and the previous studies by the same author [39-41] we can suggest the mechanism of pitting corrosion in these different steps as shown in Figure (10). The first step (a) is the formation of CuBr as in Eq. (2). Most of the formed CuBr can undergo hydrolysis as in the following reaction;

$$2CuBr + H_2O = Cu_2O + 2H^+ + 2Br^- \quad (10)$$

As shown in step (b) not all CuBr can undergo hydrolysis but a small amount of it is trapped underlying the formed Cu_2O. The trapped CuBr and the cavities or depressions, which are filled with the dense and massive carbon become weak points in the oxide passive film of Cu_2O, where Ni atom can occupy the vacancy in the Cu_2O. On the other hand, another type of the oxide film is formed at the outer most layer on the surface which is formed by hydrolysis of soluble $CuBr^-$ from solution as in Eq. (8). This type of Cu_2O film in case of the first cycle is not enough to act with the inward doped Cu_2O film for prevent the general dissolution. In the second cycle LiBr solution become saturated with $CuBr_2^-$ and accordingly Cu_2O film formed by hydrolysis as in Eq. (8) become more thick enough to act with the doped inward Cu_2O in the protection of Cu\10Ni alloy from the general dissolution and to start the pitting corrosion at the week point on the surface. As the concentration of 4M LiBr is more aggressive and enough to penetrate the Cu_2O film which cover both the trapped CuBr and the interface between the massive carbon which is considered cathodic with respect to anodic passive film of Cu_2O as in steps (c). The yield initiated pits will propagate as shown in steps (d) and (e).

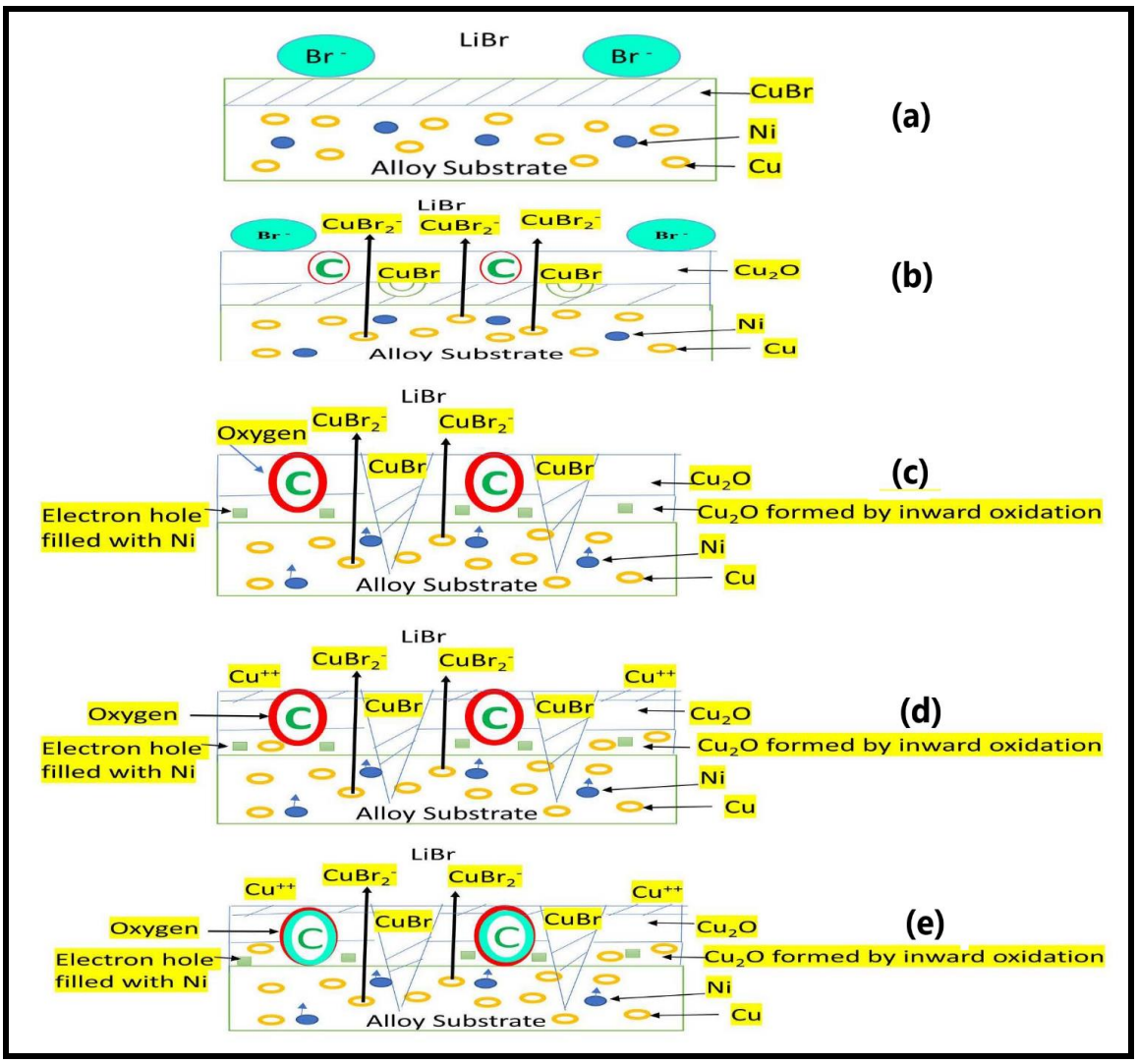

Figure 10. Schematic representation of the mechanism of pitting corrosion of Cu/10Ni in heavy brine LiBr solutions.

4. CONCLUSIONS

The anodic potentiodynamic polarization of Cu/10Ni and Al-bronze in different concentration of LiBr 4, 6 and 9 M have been studied. In 4 M LiBr, no hysteresis loop area was recorded. One step was recorded in case of Cu\10Ni at -340 mV and at low current density of 0.04 mA/cm^2, as a result of the formation of doped Cu_2O. By exchange the sample only by a new one in the same solution a hysteresis loop area was recorded in the second cyclic of anodic cyclic polarization at E_{Pit} = -135mV and I_{Pit} = 0.05 mA/cm^2. Also the hysteresis loop area appears at very small current density when taken the sample of Cu/10 Ni in 4 M LiBr solution containing the SCP of each of Cu/10Ni, Cu/30Ni, Cu/30Zn and Cu/7Al due to the formation of a protective film of doped Cu_2O with Ni. Whereas, in the cyclic polarization of Cu/10Ni in the SCP of Al-bronze in 6 M LiBr, a large hysteresis loop area is produced over a wide range of passive region from -350 to +100 mV and the current density decreased. The amount of Cu and Ni were increased by increasing the time of polarization. The ratio of Cu/Ni in solution was smaller than the ratio of the bulk alloy at all polarization periods of time due to the growth of the film on the surface and the amount of Cu^{2+} have sufficient to go to solution and precipitate as copper metal. On the other hand, the similar results were recorded in Al-bronze in 4 M LiBr but no detection of the step recorded at low current density as in Cu/10Ni. Current-time measurement of the two alloys indicated that, the initial current densities decrease at the moment of polarization then followed by a steady state. A higher steady state is occurring in case of Al-bronze and the lower steady state is recorded in Cu/10Ni. The SEM examination of the electrodes surface evidenced the presence of a large number of pit initiation and a small number of pitting propagation. This occurs as a result of formation of a protective film of doped Cu_2O on Cu/10Ni alloy surface. The oxide films formed become more compact and passive and the pitting attack occurs at small location area. The EDX analysis inside pit indicated that Cu and Ni present on the surface with very small amount while Br show a higher value inside pit than outside which confirm the role of Br^- in the pitting attack. The presences of O with a higher value than Br outside the pit suggested that the surface is covered mainly with a Cu_2O and NiO. On the other hand, SEM for the film formed on the surface of Al-bronze shows a black spots (cavity) and different type of grains such as equiaxed grain and needled or platelet likes grain. In case of Al-bronze the concentration of Br outside the cavity is higher than that recorded inside. Also, the carbon inside cavity is higher than that outside. The dealuminification of the surface is occurring either outside or inside the cavities.

ACKNOWLEDGMENT
Researchers Supporting Project number (RSP-2019/33), King Saud University, Riyadh, Saudi Arabia.

References

1. E. Samiento-Butos, J.G.G. Rodriguez, J. Uruchurtu, G. Dominguez-Patino, V.M. Salinas-Bravo, *Corros. Sci.*, 50 (2008) 2296.
2. A.I. Munoz, J.G. Anton, J.L. Guinon, V. Perez Herranz, *Corros. Sci.*, 48 (2006) 3349.

3. A.I. Munoz, J.G. Anton, J.L. Guinon, V. Perez Herranz, *Corros. Sci.*, 48 (2006) 4127.
4. E. blasco-Tamarit, A. Igual-Munoz, J. G. Anton, D. Garci-Garcia, *Corros. Sci.*, 48 (2006) 863.
5. W. Rivera, R.J. Romero, M.J. Cardoso, J. Aguillon, R. Best, *Inter. J. Ener. Res.*, 26 (2002) 747.
6. R.J. Romero, P.M.A. Basurto, H.A.H. Jimenez, M.J.J. Sanchez, *Sol. Ener.*, 80 (2006) 177.
7. D.M. Garcia-Garcia, J. Garcia-Anton, A. Lgual-Munoz, E. Blasco-Tamarit, *Corros. Sci.*, 48 (2006) 2380.
8. A.I. Munoz, J.G. Anton, J.L. Guinon, V. Perez Herranz, *Electrochim. Acta*, 50 (2004) 967.
9. A.I. Munoz, J.G. Anton, S.L. Nuevalos, J.L. Guinon, V.P. Herranz, *Corros. Sci.*, 46 (2004) 2955.
10. A. Soliz, L. Caceres, *Inter. J. Electrochem. Sci.*, 12 (2017) 7921.
11. A. Soliz, L. Caceres, *Inter. J. Electrochem. Sci.*, 10 (2015) 5673.
12. E.A. Abd El Meguid, S.S. Abd El Rehim, S.A. Al Kiey, *Corros. Eng. Sci. Technol.*, 51 (2016) 429.
13. R. M. Fernandez-Domene, E. Blasco-Tamarit, D.M. Garcia-Garcia, J. Garcia-Anton, *Thin Solid Films*, 558 (2014) 253.
14. A.L. Ma, S.L. Jiang, Y.G. Zheng, W. Ke, *Corros. Sci.*, 91 (2015) 245
15. W. Schleich, *EuroCorr 2004, NACE*, 1-10, (2004).
16. S.A. Campbell, G.J.W. Radford, C.D.S. Tuck, B.D. Barker, *Corroion*, 58 (2002) 57.
17. R.C.V. Liberto, R. Magnabosco, N. Alonso-Faileiros, *Corrosion*, 63 (2007) 211.
18. R. F. North, M. J. Pryor, *Corros. Sci.*, 10 (1970) 297.
19. A.A. El Warraky, A.E. El Meleigy, Sh.E. Abd El Hamid, *Egypt. J. Chem.*, 59 (5) (2016) 833.
20. G.I. Youssef, M.F. Shehata, A.E. Meleigy, A.A. Warraky, A.M.A. Aziz, *Ochrona Przed Korozja (Corros. Prot.)*, nr 2 (2013) 34.
21. A.E. El Meleigy, Sh.E. Abd El Hamid, A.A. El Warraky, *Brit. J. Appl. Sci. Technol.*, 11 (2015) 1.
22. A.E. El Meleigy, M.F. Shehata, G.I. Youssef, Sh.E. Abd El Hamid, A.A. El Warraky, *Ochrona Przed Korozja (Corros. Prot.) nr 10 (*2012) 427.
23. C.N. Cao, Principles of Electrochemistry of corrosion ,3rd ed., *Chemical Industry Press*, China, (2008).
24. A.A. El Warraky, *Brit. Corros. J.*, 32 (1997) 57.
25. T.M.H. Saber and A.A. El Warraky, *J. Mater. Sci.*, 23 (1988) 1496.
26. G. Remond, P.H. Holloway, C.T. Hovland, R.R. Olson, *Scanning Electron Microscopy* "111 (SEM Inc, AMF O Hare, Chicago, USA, (1982) 995.
27. Zhu Xiaolong, Lei Tingquan, *Corros. Sci.*, 44 (2002) 67-79.
28. J.E. Castle, M.S. Parvizi, *Corros. Prev. Control*, 17(1) (1986) 1.
29. G. Kear, B.D. Barker, F.C. Walsh, *Corros. Sci.*, 46 (2004) 109.
30. J. Mathiyarasu, N. Palaniswamy, V.S. Muralidharan, *Proc. India Acad. Sci. (Chem. Sci.)*, 111 (1999) 377.
31. R.J.K. Wood, S.P. Hutton, D.J. Schiffrin, *Corros. Sci*., 30 (1990) 1177.
32. G. Kear, B.D. Barker, K.R. Stokes, F.C. Walsh, *Electrochim. Acta*, 52 (2007) 2343.
33. G. Bianchi, G. Fioro, P. Longhi, F. Mazza, *Corrosion*, 34 (1978) 396.
34. H.P. Dhar, R.E. White G. Burnell, L.R. Cornwell, R.B. Griffin R. Darby, *Corrosion*, 41(1985) 317.
35. W.J. Ooij Van, *Surf. Technol*., 6 (1997) 1.
36. T.M. H. Saber and A.A. El Warraky, *Desalination*, 93 (1993) 473.
37. A.A. El Warraky, A.E. El Meleigy, *Brit. Corros. J.*, 37 (2002) 1.
38. A.E. El Meleigy, El Warraky, A.A., *Corros. Eng. Sci. Technol.*, 38 (2013) 218.
39. A.A. El Warraky, H.A. El Shayeb, and E.M. Sherif, *Anti- Corros. Method. Mater*., 51 (2004) 52.
40. A.A. El Warraky, H.A. El Shayeb, and E.M. Sherif, *Egypt. J. Chem.*, 47 (2004) 657.
41. A.A. El Warraky, H.A. El Shayeb, and E.M. Sherif, *Egypt. J. Chem.*, 47 (2004) 609.

© 2020 The Authors. Published by ESG (www.electrochemsci.org). This article is an open access article distributed under the terms and conditions of the Creative Commons Attribution license (http://creativecommons.org/licenses/by/4.0/).